RESEARCH ARTICLE
SPACE PHYSICS: MAGNETOSPHERIC PHYSICS

Earth and Planetary Physics
3: 305–313, 2019
doi: 10.26464/epp2019032

Poleward-moving recurrent auroral arcs associated with impulse-excited standing hydromagnetic waves

HuaYu Zhao[1], Xu-Zhi Zhou[1]*, Ying Liu[1], Qiu-Gang Zong[1], Robert Rankin[2], YongFu Wang[1], QuanQi Shi[3], Xiao-Chen Shen[4], Jie Ren[1], Han Liu[1], and XingRan Chen[1]

[1]School of Earth and Space Sciences, Peking University, Beijing 100871, China;

[2]Department of Physics, University of Alberta, Edmonton, Alberta T6G2J1, Canada;

[3]School of Space Science and Physics, Shandong University, Weihai 264209, China;

[4]Center for Space Physics, Boston University, Boston, Massachusetts 02215, USA

Abstract: In Earth's high-latitude ionosphere, the poleward motion of east–west elongated auroral arcs has been attributed to standing hydromagnetic waves, especially when the auroral arcs appear quasi-periodically with a recurrence time of a few minutes. The validation of this scenario requires spacecraft observations of ultra-low-frequency hydromagnetic waves in the magnetosphere and simultaneous observations of poleward-moving auroral arcs near the spacecraft footprints. Here we present the first observational evidence from the multi-spacecraft THEMIS (Time History of Events and Macroscale Interactions during Substorms) mission and the conjugated all-sky imager to support the scenario that standing hydromagnetic waves can generate the quasi-periodic appearance of poleward-moving auroral arcs. In this specific event, the observed waves were toroidal branches of the standing hydromagnetic waves, which were excited by a pulse in the solar wind dynamic pressure. Multi-spacecraft measurements from THEMIS also suggest higher wave frequencies at lower L shells (consistent with the distribution of magnetic field line eigenfrequencies), which indicates that the phase difference across latitudes would increase with time. As time proceeds, the enlarged phase difference corresponds to a lower propagation speed of the auroral arcs, which agrees very well with the ground-based optical data.

Keywords: poleward-moving auroral arcs; ULF waves; standing hydromagnetic waves; field-aligned currents; solar wind dynamic pressure pulse

Citation: Zhao, H. Y., Zhou, X.-Z., Liu, Y., Zong, Q.-G., Rankin, R., Wang, Y. F., Shi, Q. Q., Shen X.-C., Ren, J., Liu, H., and Chen, X. R. (2019). Poleward-moving recurrent auroral arcs associated with impulse-excited standing hydromagnetic waves. *Earth Planet. Phys.*, *3*(4), 305–313. http://doi.org/10.26464/epp2019032

1. Introduction

In the high-latitude ionosphere, the quasi-periodic appearance of poleward-moving auroral arcs (PMAAs) has attracted considerable research interest (e.g., Samson et al., 1996; Milan et al., 1999, 2001; Kozlovsky and Kangas, 2002; Rankin et al., 2005). This specific type of auroral arc is usually elongated in the east–west direction, which propagates poleward at a typical velocity of 150–300 m/s and appears quasi-periodically with a recurrence time of a few minutes (Milan et al., 2001; Kozlovsky and Kangas, 2002).

In the past decades, the generation and poleward propagation of auroral arcs on closed geomagnetic field lines have been attributed to the ultra-low-frequency (ULF) hydromagnetic wave activities associated with field line resonances (FLRs). The resonance of geomagnetic field lines enables standing ULF waves to form at a frequency close to the field line eigenfrequency (Chen L and Hasegawa, 1974; Southwood, 1974; Mann, 1997; Hartinger et al., 2011; Zong QG et al., 2017), which accelerates electrons into the ionosphere to form auroral arcs (Hasegawa, 1976; Greenwald and Walker, 1980; Lyatsky et al., 1999; Rae et al., 2005; Rankin et al., 2005). Milan et al. (1999, 2001) reported that the PMAAs show clear characteristics of FLRs and that the recurrence frequency is consistent with observations of geomagnetic pulsations. These observations suggest a close correlation between FLRs and PMAAs.

In the theoretical framework developed by Greenwald and Walker (1980) and Milan et al. (2001), the PMAAs reflect the distributions of FLR-associated field-aligned currents (FACs). In a region with upward FACs, the downward-moving electrons could be accelerated by a parallel electric field (which appears if the electron flow exceeds a certain threshold magnitude) and result in auroral luminosity enhancements. Interested readers may refer to Stasiewicz et al. (2000) for a review of the relationships among FACs, parallel electric fields, and small-scale auroral arcs.

To better illustrate the poleward motion of auroral arcs in the presence of geomagnetic pulsations, one may follow the scenario proposed by Greenwald and Walker (1980) to estimate the latitudinal distribution of FACs (as the proxy to variations in auroral lu-

Correspondence to: X. Z. Zhou, xuzhi.zhou@gmail.com
Received 18 APR 2019; Accepted 03 JUN 2019.
Accepted article online 14 JUN 2019.

minosity) associated with standing ULF waves. Here the magnetic field perturbations above the ionosphere are assumed to be in the azimuthal direction (i.e., we focus on the toroidal branch of hydromagnetic waves), with the wave field profile (at a fixed longitude) given by

$$B_y \propto G(t,x)\cos\left[\omega t+\phi_0(x)\right], \tag{1}$$

in which the x direction points poleward, the z direction points vertically upward (which is nearly parallel or antiparallel, depending on the hemisphere, to the geomagnetic field lines), and the azimuthal y direction completes the triad. In the standard FLR model (Kivelson and Southwood, 1985; Samson et al., 1992), the ULF waves are confined within a certain region where the field line eigenfrequencies are close to the driver frequencies. In other words, the wave frequency ω in equation (1) is constant within the wave active region (with its spatial and temporal extents given by $G(t, x)$). The wave-associated FACs can then be calculated based on Ampère's law:

$$J_z=\frac{1}{\mu_0}\frac{\partial B_y}{\partial x}=\frac{1}{\mu_0}\left[G'\cos\left(\omega t+\phi_0\right)-G\phi_0{}'\sin\left(\omega t+\phi_0\right)\right], \tag{2}$$

where G' represents the partial derivative of $G(t,x)$ with respect to x, and ϕ_0' is the gradient of $\phi_0(x)$. Therefore, in this simplistic model, the wave-associated FACs and magnetic fields both clearly show quasi-periodic oscillations.

Figure 1 provides two examples of the wave-carried magnetic field (as solid lines) and FAC perturbations (as colored patches), which are shown as functions of time and latitude. In Figure 1a, the ULF waves are assumed to be excited first at low latitudes (small L shells) and then propagate to high latitudes (large L shells). In this case, upward FACs (i.e., positive $\frac{\partial B_y}{\partial x}$ values) appear

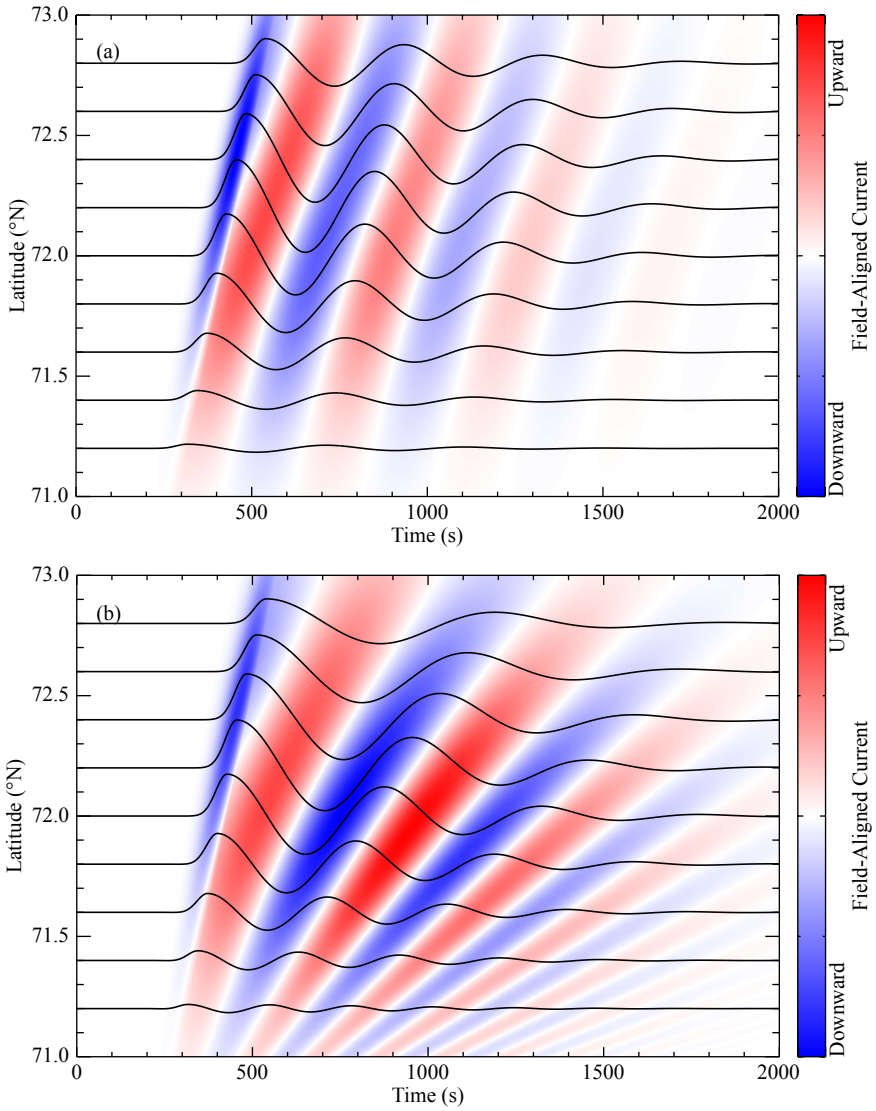

Figure 1. Schematic illustration of the latitudinal–temporal evolution of field-aligned currents (FACs) in toroidal-mode standing hydromagnetic waves. The black lines represent the azimuthal magnetic field oscillations, and the red and blue stripes correspond to the regions with upward and downward FACs, respectively. (a) In the model with a fixed wave frequency, the FAC stripes propagate at a constant speed. (b) In the model in which the wave frequency depends on the latitude, the propagation speed of the FAC stripes changes with time.

mostly during the descending stages of the magnetic field oscillations, and the phase shift of the waves across latitudes corresponds to the poleward motion of the auroral arcs. When given a latitude-independent wave frequency, the phase shift and, consequently, the propagation speed of the auroral arcs hardly change with time or location. However, if the ULF wave frequency is locally determined by field line eigenfrequencies (see the observations in Sarris et al., 2009, 2010), the wave frequency ω in equation (1) would gradually decrease with increasing latitude. In this case, the phase shift across latitudes would increase with time, which corresponds to the decreasing propagation speed of the auroral arcs shown in Figure 1b.

However, the aforementioned scenario has not yet been fully established, partially because conjugate magnetospheric and ionospheric observations for PMAAs are lacking. In this paper, we present the first observations of PMAAs associated with standing hydromagnetic waves in the magnetosphere, which serve as direct evidence supporting the scenario of PMAA formation and enable better insights into the nature of ULF waves in the coupled system of Earth's magnetosphere and ionosphere.

2. Data Presentation

The solar wind and interplanetary magnetic field (IMF) measurements were obtained from the WIND satellite (Farrell et al., 1995; Gloeckler et al., 1995) and, for comparison purposes, the spacecraft-interspersed near-Earth solar wind data (OMNI data, courtesy of NASA's Space Physics Data Facility). The magnetospheric observations are available from the THEMIS (Time History of Events and Macroscale Interactions during Substorms) spacecraft (Angelopoulos, 2008), which include the spin-fit magnetic field data from a fluxgate magnetometer (Auster et al., 2008) and the plasma measurements from an electrostatic analyzer (McFadden et al., 2008). The aurora data used in this paper were derived from the all-sky imager at the Inuvik station in northern Canada, which has a 180° field of view and a resolution of 512 pixels×512 pixels.

3. Observations

On 18 January 2009, an isolated pulse of the solar wind dynamic pressure occurred at 14:16 universal time (UT). The solar wind dynamic pressure and the three IMF components in geocentric solar magnetospheric (GSM) coordinates, observed by the WIND satellite in the solar wind at GSM (222.4, −97.7, −2.7) R_E, are shown in Figure 2a and 2b. Associated with the pressure pulse, the IMF directions changed sharply, indicating the presence of a solar wind discontinuity. The near-Earth OMNI data, given in Figure 2c and 2d, show profiles very similar to those of the WIND observations except for a time shift of approximately 42 min.

When the solar wind discontinuity arrived at the magnetosphere, three THEMIS satellites (THEMIS A [THA], THEMIS D [THD], and THEMIS E [THE]) were closely clustered in the dawnside magnetosphere. Their locations in GSM coordinates were (−4.1, −9.6, −2.6) R_E, (−3.7, −9.5, −1.4) R_E, and (−4.8, −9.7, −2.0) R_E, respectively. The THEMIS three-spacecraft observations of plasma bulk velocity and magnetic field presented in Figure 3 show quasi-sinusoidal wave signatures soon after the arrival of the pressure pulse. We next define the field-aligned coordinates based on a 15-min window for the background magnetic field (e.g., Hartinger et al., 2011), in which the parallel (*p*) direction is along the background magnetic field, the azimuthal (*a*) direction is perpendicular to the background field and pointing eastward, and the radial (*r*) direction

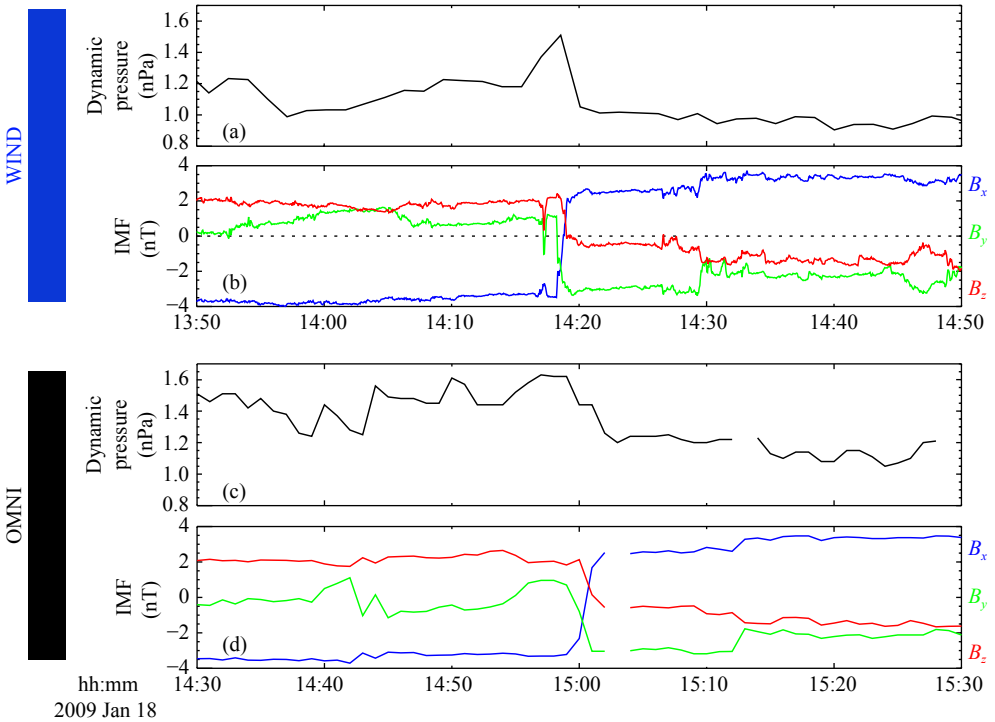

Figure 2. Solar wind dynamic pressure and interplanetary magnetic field (IMF) measurements from the (a, b) WIND satellite and from the (c, d) near-Earth OMNI data.

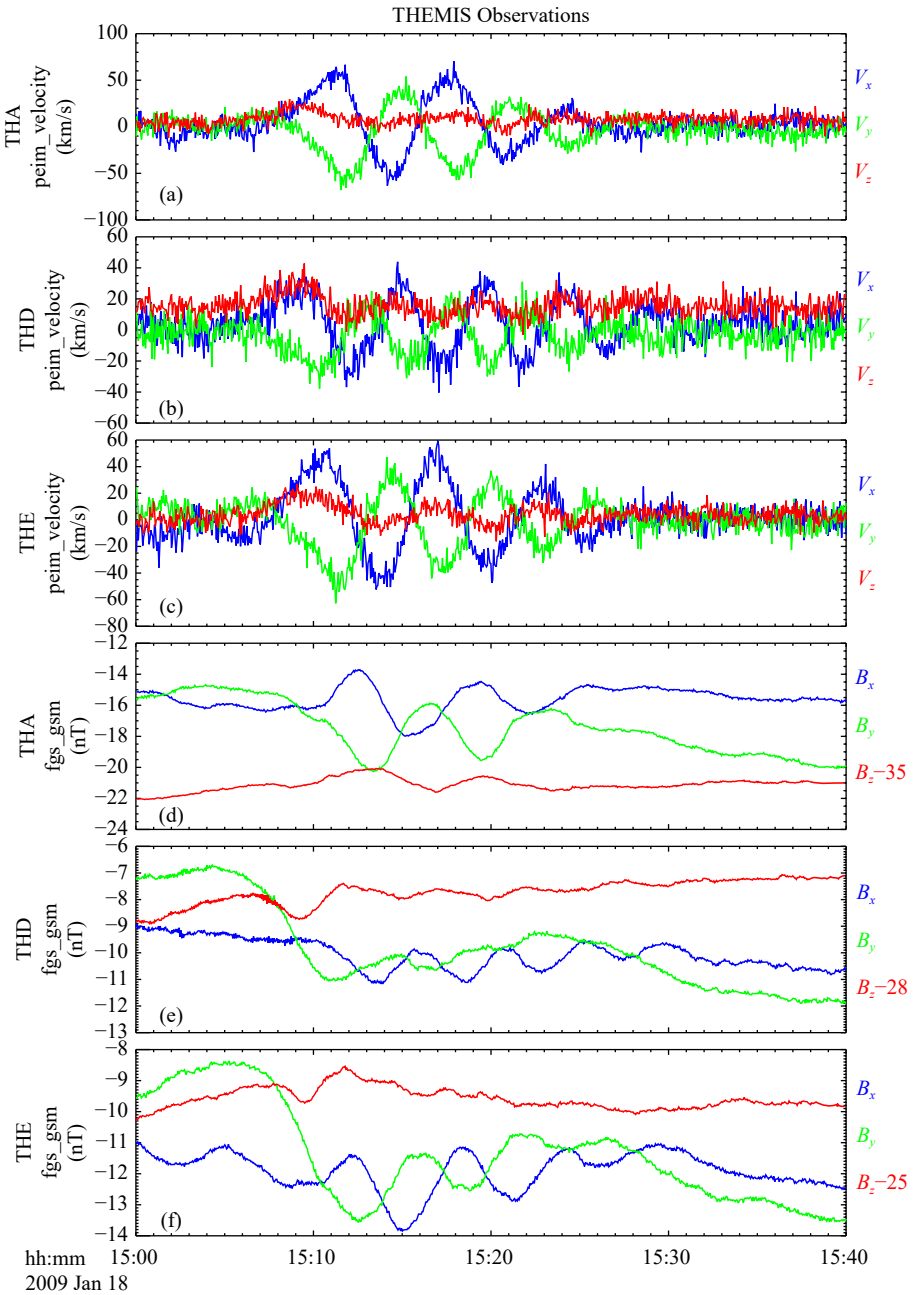

Figure 3. THEMIS observations of the ultra-low-frequency magnetic field and plasma flow perturbations. (a–c) Plasma bulk velocities observed by the THEMIS A (THA), THEMIS D (THD), and THEMIS E (THE) spacecraft. (d–f) Magnetic field measurements made by the THA, THD, and THE spacecraft. Here the observed Bz components are subtracted by 35 nT, 28 nT and 25 nT, respectively, to have three magnetic components fit in respective panels.

completes the triad. The observed magnetic and electric fields (obtained via $-V \times B$) are then transformed into the field-aligned coordinates presented in Figure 4. In all three spacecraft measurements, the quasi-sinusoidal magnetic field perturbations are clearly more significant in the azimuthal direction than in the radial direction, and the electric field perturbations are mostly in the radial direction. The phase difference between the radial electric field and the azimuthal magnetic field oscillations was approximately 90°, which indicates the dominance of standing toroidal waves. Figure 4 also shows the wavelet power spectra for the azimuthal magnetic field oscillations at the three spacecraft. The wave power peaks at 2.3 mHz, 3.5 mHz, and 2.7 mHz for the THA, THD, and THE observations, respectively.

The magnetic footprints of the THEMIS satellites in the northern hemisphere are shown in Figure 5. Here the magnetic mapping was carried out based on the T96 model (Tsyganenko and Stern, 1996) with realistic solar wind and IMF parameters. The grids in Figure 5 are given in AACGM (altitude-adjusted corrected geomagnetic) coordinates (Baker and Wing, 1989), with latitudes ranging from 50° to 70°. The latitudinal and longitudinal grid sizes are 5° and 15°, respectively. According to Figure 5, the footprints of the THEMIS satellites were all located within the field of view of the Inuvik all-sky imager (the magenta circle).

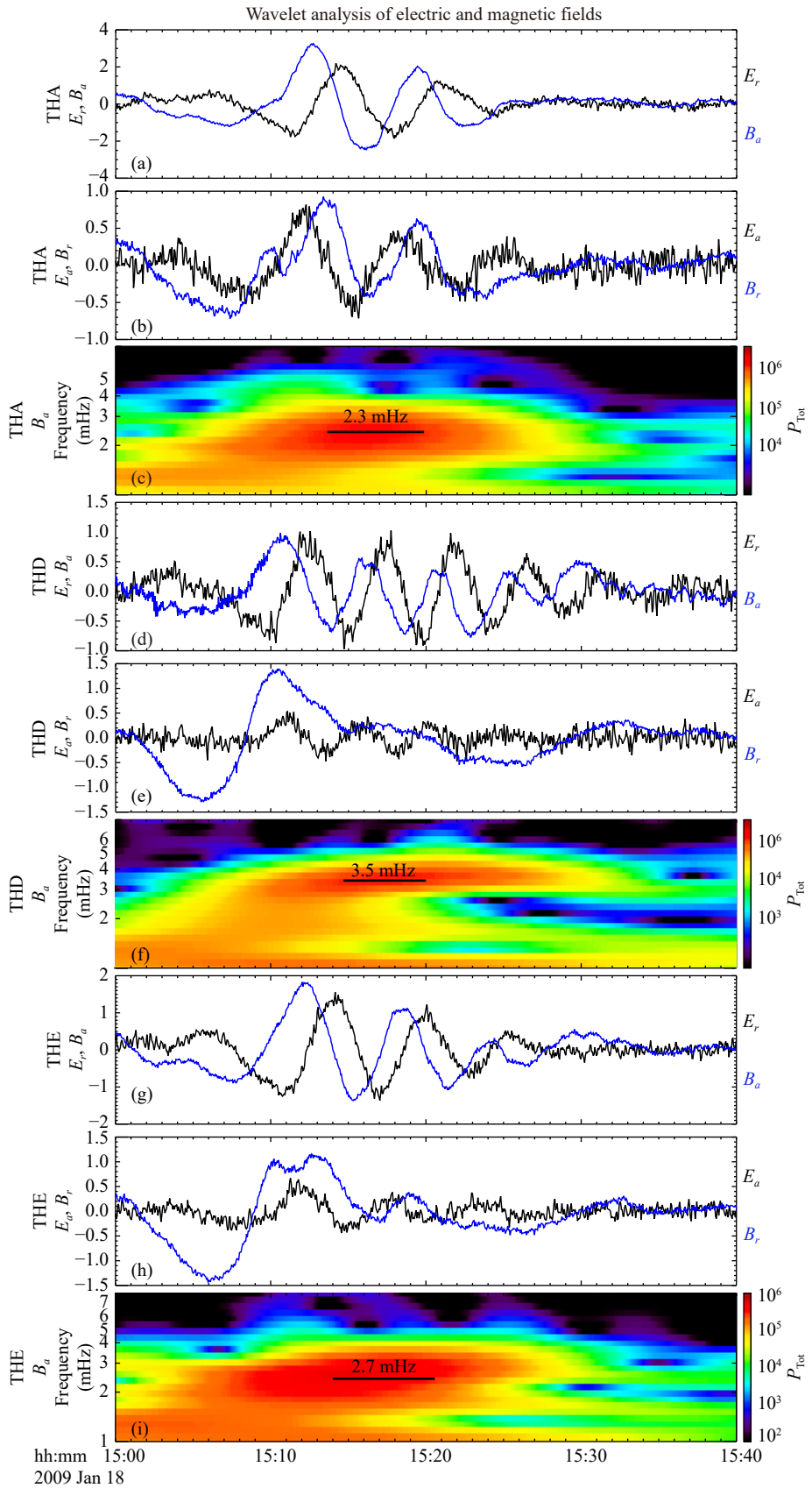

Figure 4. THEMIS A (THA), D (THD), and E (THE) observations of the electric and magnetic field variations in the field-aligned coordinates. (a, d, g) Azimuthal magnetic field and radial electric field perturbations, which correspond to the toroidal-mode ultra-low-frequency waves. (b, e, h) Radial magnetic field and azimuthal electric field perturbations, which correspond to the poloidal-mode waves. (c, f, i) Wavelet power spectra of the azimuthal magnetic field perturbations, in which the solid black lines indicate the frequencies with maximum power.

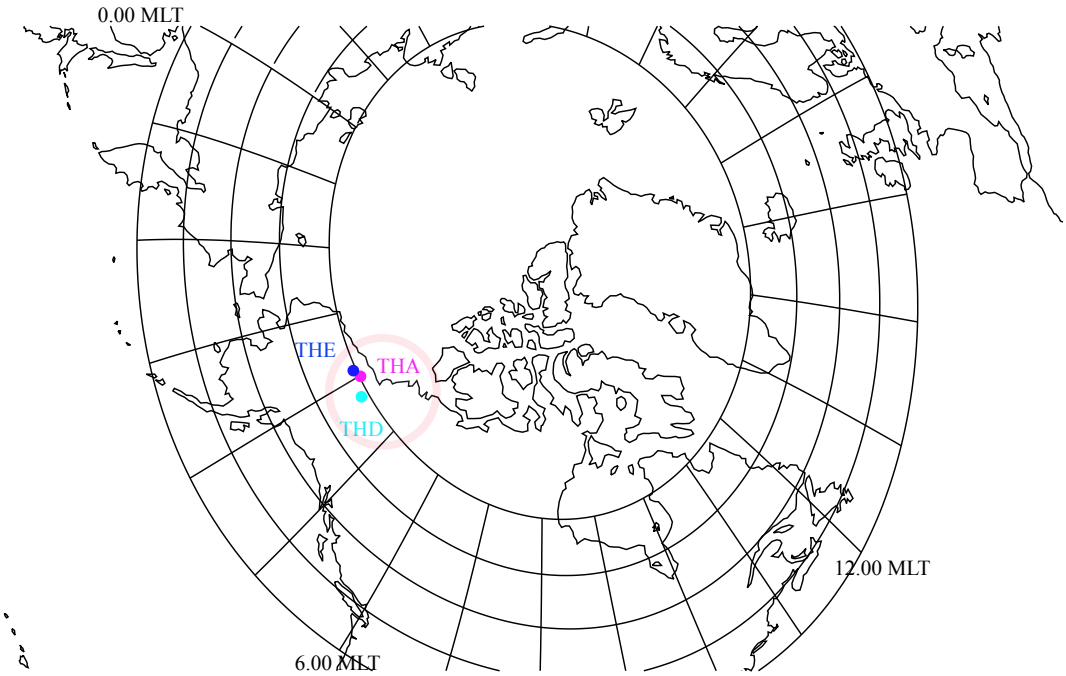

Figure 5. The magnetic footprints of the THEMIS satellites in the northern hemisphere. The magenta circle indicates the field of view of the Inuvik all-sky imager.

From the Inuvik all-sky imager, we show in Figure 6 the selected time sequence of auroral images from 15:12 to 15:38 UT. The auroral images are displayed with west to the left and south on the bottom. At ~15:14 UT, an east–west elongated auroral arc began to form, which moved poleward with increasing luminosity. At ~15:20 UT, another east–west elongated, poleward-moving arc began to form, which coexisted with the former arc before the two arcs faded out at ~15:25 and ~15:32 UT, respectively. A third poleward-moving arc was also present between ~15:29 and ~15:36 UT, although its luminosity was less significant than those of the former arcs. The progression of auroral activity is also presented as a keogram in the bottom panel of Figure 6, which shows the auroral intensity as a function of magnetic latitude and time. From this keogram, one may calculate the average poleward speed of the auroral arcs as 0.5 km/s, although a clear trend was also that the speed decreased with time. One may also estimate the latitudinal widths of the auroral arcs and the inter-arc separations (which are most accurate when the arc/gap has passed the zenith of the imager field of view) as ~20 km and ~130 km, respectively. These characteristics are very similar to those reported by Samson et al. (2003). More interesting, it is evident from the keogram that the poleward-moving arcs appeared quasi-periodically, which coincided in space and time with the toroidal-mode ULF waves shown in Figures 3 and 4. From Figure 6 one may also determine the recurrent frequency of the auroral arcs as being in the range of 1.9–2.3 mHz (depending on the magnetic latitude), which is consistent with the ULF wave observations.

4. Discussion

We next utilized the model by Rankin et al. (2006) to show that the ULF wave frequencies observed by the THEMIS satellites matched the geomagnetic field line eigenfrequencies under the observed solar wind and magnetospheric conditions. The input parameters for the model included the solar wind dynamic pressure, 1.1 nPa; *Dst* (disturbance storm time) index, –5 nT; the IMF *x* and *y* components, –3 nT and –0.5 nT; the plasma density, 0.34 (THA), 0.41 (THD), 0.39 (THE); and the L shells, 12.95 (THA), 10.75 (THD), 12.28 (THE). The model yielded eigenfrequencies of 2.4 mHz, 3.5 mHz, and 2.6 mHz for the magnetic field lines threading THA, THD, and THE, respectively. These eigenfrequencies were almost identical to the observed ULF wave frequencies (2.3 mHz, 3.5 mHz, and 2.7 mHz; see Figure 4).

In other words, the magnetospheric ULF wave frequency was not determined by a global driver in this event (such as the cavity mode or magnetopause surface waves; see the FLR models in Kivelson and Southwood, 1985, and Samson et al., 1992). Instead, the observed waves were hydromagnetic waves standing on their respective field lines. This could be because the observed ULF waves were triggered by a solar wind pressure pulse, which provided a broadband energy source in the frequency domain for the excitation of standing waves at the respective eigenfrequencies. In fact, the outermost and innermost THEMIS spacecraft, THA and THD, observed the lowest (2.4 mHz) and the highest (3.5 mHz) wave frequencies, respectively. These features also agree with the expectation of decreasing frequencies at increasing L shells (or, equivalently, latitudes). Therefore, the scenario given in Figure 1b (rather than Figure 1a) applies in this event. As discussed in the Introduction, this latitude-dependent wave frequency results in an increasing phase shift across latitudes as time proceeds, which indicates a gradual decrease in the wave phase velocity in the poleward direction. Therefore, one would expect an auroral keogram similar to Figure 1b, with the increasingly tilted red and blue stripes corresponding to the upward and downward FAC regions with enhanced and reduced auroral luminosity. This result is very

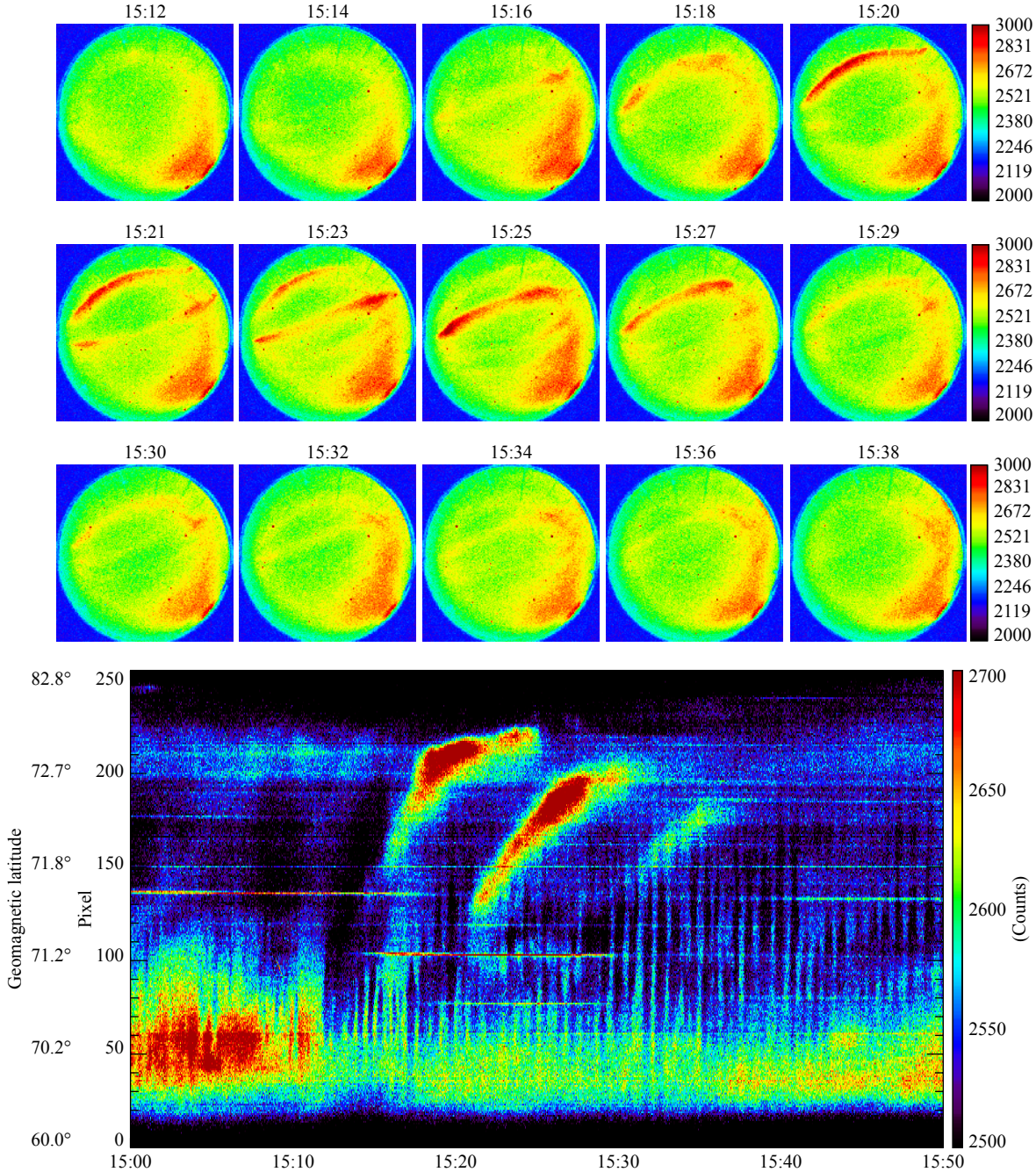

Figure 6. Auroral observations from the Inuvik station. The upper panels show the selected time sequence of the auroral images from the all-sky camera, displayed with west to the left and south on the bottom. The bottom panel shows the keogram of auroral brightness as a function of time and latitude during the interval between 15:00 and 15:50 UT.

consistent with the auroral observations in Figure 6. Moreover, we noted that the damping of the ULF waves in Figure 1b (which could be modeled by a Gaussian envelope of the wave amplitude; see Zhou XZ et al., 2016) corresponded to the gradual fading of the auroral pattern. This image is also supported by the observations of damping ULF waves in Figure 4 and fading auroral arcs in Figure 6.

5. Summary

In this study, we used multiple-instrument observations to investigate the quasi-periodic appearance of PMAAs in association with standing hydromagnetic waves in the dawnside magnetosphere, which occurred soon after the impact of a solar wind dynamic pressure pulse on 18 February 2009. To our knowledge, this is the first study on the formation of PMAAs that includes all evidence from solar wind, magnetospheric, and ground-based optical observations.

In this specific event, the three THEMIS satellites observed strong ULF wave activities, identified as toroidal-mode hydromagnetic waves standing on their respective field lines. The wave frequen-

cies were very close to the eigenfrequencies of the magnetic field lines threading the satellites, which showed a clear decreasing trend for increasing L shells. Near the magnetic footprints of the THEMIS satellites, the all-sky imager at the Inuvik station observed a series of recurrent PMAAs. The poleward speed of the auroral arcs, which averaged 0.5 km/s, clearly decreased with time. These observational characteristics are all consistent with a simple model of FACs carried by toroidal ULF waves (estimated based on the curl of the wave magnetic field). In this model, the latitude dependence of the ULF wave frequency contributes to the increasing phase shift across latitudes, which in turn can manifest as the decreasing propagation speed of the auroral arcs.

In addition to showing a strong association between the magnetospheric ULF waves and quasi-periodic auroral arcs, the results of this study suggest that different drivers of the ULF waves may correspond to different auroral signatures. In this event, the ULF waves were triggered by a broadband source in the frequency domain (a sudden pulse of solar wind dynamic pressure), which enabled the excitation of ULF waves with different frequencies at different locations. As discussed above, this is the reason the auroral arcs propagate poleward at a decreasing speed. If the ULF waves were triggered by a more monochromatic global source (such as the magnetospheric cavity mode, surface waves, or both), a more constant speed of the auroral motion would be expected. This expectation will be examined in a future study.

Acknowledgments

We acknowledge V. Angelopoulos for the use of data from the THEMIS mission. Specifically, we thank C. W. Carlson and J. P. McFadden for the electrostatic analyzer data; K. H. Glassmeier, U. Auster, and W. Baumjohann for the flux gate magnetometer data; and S. Mende and E. Donovan for the THEMIS all-sky imager data. All the THEMIS data can be obtained from http://themis.ssl.berkeley.edu/data/themis/. The authors thank the Coordinated Data Analysis Web (CDAWeb) for providing the WIND and OMNI data. This study was supported by the National Natural Science Foundation of China (grant numbers 41774168 and 41421003).

References

Angelopoulos, V. (2008). The THEMIS mission. *Space Sci. Rev.*, *141*(1-4), 5–34. https://doi.org/10.1007/s11214-008-9336-1

Auster, H. U., Glassmeier, K. H., Magnes, W., Aydogar, O., Baumjohann, W., Constantinescu, D., Fischer, D., Fornacon, K. H., Georgescu, E., … Wiedemann, M. (2008). The THEMIS fluxgate magnetometer. *Space Sci. Rev.*, *141*(1-4), 235–264. https://doi.org/10.1007/s11214-008-9365-9

Baker, K. B., and Wing, S. (1989). A new magnetic coordinate system for conjugate studies at high latitudes. *J. Geophys. Res.*, *94*(A7), 9139–9143. https://doi.org/10.1029/JA094iA07p09139

Chen, L., and Hasegawa, A. (1974). A theory of long-period magnetic pulsations: 2. Impulse excitation of surface eigenmode. *J. Geophys. Res.*, *79*(7), 1033–1037. https://doi.org/10.1029/JA079i007p01033

Farrell, W. M., Thompson, R. F., Lepping, R. P., and Byrnes, J. B. (1995). A method of calibrating magnetometers on a spinning spacecraft. *IEEE Trans. Magn.*, *31*(2), 966–972. https://doi.org/10.1109/20.364770

Gloeckler, G., Balsiger, H., Bürgi, A., Bochsler, P., Fisk, L. A., Galvin, A. B., Geiss, J., Gliem, F., Hamilton, D. C., … Wilken, B. (1995). The solar WIND and suprathermal ion composition investigation on the wind spacecraft. *Space Sci. Rev.*, *71*(1-4), 79–124. https://doi.org/10.1007/BF00751327

Greenwald, R. A., and Walker, A. D. M. (1980). Energetics of long period resonant hydromagnetic waves. *Geophys. Res. Lett.*, *7*(10), 745–748. https://doi.org/10.1029/GL007i010p00745

Hartinger, M., Angelopoulos, V., Moldwin, M. B., Glassmeier, K. H., and Nishimura, Y. (2011). Global energy transfer during a magnetospheric field line resonance. *Geophys. Res. Lett.*, *38*(12), L12101. https://doi.org/10.1029/2011GL047846

Hasegawa, A. (1976). Particle acceleration by MHD surface wave and formation of aurora. *J. Geophys. Res.*, *81*(28), 5083–5090. https://doi.org/10.1029/JA081i028p05083

Kivelson, M. G., and Southwood, D. J. (1985). Resonant ULF waves: a new interpretation. *Geophys. Res. Lett.*, *12*(1), 49–52. https://doi.org/10.1029/GL012i001p00049

Kozlovsky, A., and Kangas, J. (2002). Motion and origin of noon high-latitude poleward moving auroral arcs on closed magnetic field lines. *J. Geophys. Res.*, *107*(A2), 1017. https://doi.org/10.1029/2001JA900145

Lyatsky, W., Elphinstone, R. D., Pao, Q., and Cogger, L. L. (1999). Field line resonance interference model for multiple auroral arc generation. *J. Geophys. Res.*, *104*(A1), 263–268. https://doi.org/10.1029/1998JA900027

Mann, I. R. (1997). On the internal radial structure of field line resonances. *J. Geophys. Res.*, *102*(A12), 27109–27119. https://doi.org/10.1029/97JA02385

McFadden, J. P., Carlson, C. W., Larson, D., Ludlam, M., Abiad, R., Elliott, B., Turin, P., Marckwordt, M., and Angelopoulos, V. (2008). The THEMIS ESA plasma instrument and in-flight calibration. *Space Sci. Rev.*, *141*(1-4), 277–302. https://doi.org/10.1007/s11214-008-9440-2

Milan, S. E., Yeoman, T. K., Lester, M., Moen, J., and Sandholt, P. E. (1999). Post-noon two-minute period pulsating aurora and their relationship to the dayside convection pattern. *Ann. Geophys.*, *17*(7), 877–891. https://doi.org/10.1007/s00585-999-0877-8

Milan, S. E., Sato, N., Ejiri, M., and Moen, J. (2001). Auroral forms and the field-aligned current structure associated with field line resonances. *J. Geophys. Res.*, *106*(A11), 25825–25833. https://doi.org/10.1029/2001JA900077

Rae, I. J., Donovan, E. F., Mann, I. R., Fenrich, F. R., Watt, C. E. J., Milling, D. K., Lester, M., Lavraud, B., Wild, J. A., … Balogh, A. (2005). Evolution and characteristics of global Pc5 ULF waves during a high solar wind speed interval. *J. Geophys. Res.*, *110*(A12), A12211. https://doi.org/10.1029/2005JA011007

Rankin, R., Kabin, K., Lu, J. Y., Mann, I. R., Marchand, R., Rae, I. J., Tikhonchuk, V. T., and Donovan, E. F. (2005). Magnetospheric field-line resonances: ground-based observations and modeling. *J. Geophys. Res.*, *110*(A10), A10S09. https://doi.org/10.1029/2004JA010919

Rankin, R., Kabin, K., and Marchand, R. (2006). Alfvénic field line resonances in arbitrary magnetic field topology. *Adv. Space Res.*, *38*(8), 1720–1729. https://doi.org/10.1016/j.asr.2005.09.034

Samson, J. C., Harrold, B. G., Ruohoniemi, J. M., Greenwald, R. A., and Walker, A. D. M. (1992). Field line resonances associated with MHD waveguides in the magnetosphere. *Geophys. Res. Lett.*, *19*(5), 441–444. https://doi.org/10.1029/92GL00116

Samson, J. C., Cogger, L. L., and Pao, Q. (1996). Observations of field line resonances, auroral arcs, and auroral vortex structures. *J. Geophys. Res.*, *101*(A8), 17373–17383. https://doi.org/10.1029/96JA01086

Samson, J. C., Rankin, R., and Tikhonchuk, V. T. (2003). Optical signatures of auroral arcs produced by field line resonances: comparison with satellite observations and modeling. *Ann. Geophys.*, *21*(4), 933–945. https://doi.org/10.5194/angeo-21-933-2003

Sarris, T. E., Liu, W., Kabin, K., Li, X., Elkington, S. R., Ergun, R., Rankin, R., Angelopoulos, V., Bonnell, J., … Auster, U. (2009). Characterization of ULF pulsations by THEMIS. *Geophys. Res. Lett.*, *36*(4), L04104. https://doi.org/10.1029/2008GL036732

Sarris, T. E., Liu, W., Li, X., Kabin, K., Talaat, E. R., Rankin, R., Angelopoulos, V., Bonnell, J., and Glassmeier, K. H. (2010). THEMIS observations of the spatial extent and pressure-pulse excitation of field line resonances. *Geophys. Res. Lett.*, *37*(15), L15104. https://doi.org/10.1029/2010GL044125

Southwood, D. J. (1974). Some features of field line resonances in the magnetosphere. *Planet. Space Sci.*, *22*(3), 483–491.

https://doi.org/10.1016/0032-0633(74)90078-6

Stasiewicz, K., Bellan, P., Chaston, C., Kletzing, C., Lysak, R., Maggs, J., Pokhotelov, O., Seyler, C., Shukla, P., … Wahlund, J. E. (2000). Small scale Alfvénic structure in the aurora. *Space Sci. Rev.*, *92*(3-4), 423–533. https://doi.org/10.1023/A:1005207202143

Tsyganenko, N. A., and Stern, D. P. (1996). Modeling the global magnetic field of the large-scale Birkeland current systems. *J. Geophys. Res.*, *101*(A12), 27187–27198. https://doi.org/10.1029/96JA02735

Zhou, X. Z., Wang, Z. H., Zong, Q. G., Rankin, R., Kivelson, M. G., Chen, X. R., Blake, J. B., Wygant, J. R., and Kletzing, C. A. (2016). Charged particle behavior in the growth and damping stages of ultralow frequency waves: theory and Van Allen Probes observations. *J. Geophys. Res.*, *121*(4), 3254–3263. https://doi.org/10.1002/2016JA022447

Zong, Q. G., Rankin, R., and Zhou, X. Z. (2017). The interaction of ultra-low-frequency Pc3-5 waves with charged particles in Earth's magnetosphere. *Rev. Mod. Plasma Phys.*, *1*, 10. https://doi.org/10.1007/s41614-017-0011-4